



Anthropogenic
bioavailable Fe
deposition

A. Ito and Z. Shi

This discussion paper is/has been under review for the journal Atmospheric Chemistry and Physics (ACP). Please refer to the corresponding final paper in ACP if available.

Delivery of anthropogenic bioavailable iron from mineral dust and combustion aerosols to the ocean

A. Ito¹ and Z. Shi²

¹Yokohama Institute for Earth Sciences, JAMSTEC, Yokohama, Kanagawa, Japan

²School of Geography, Earth and Environmental Sciences, University of Birmingham, Birmingham, UK

Received: 30 June 2015 – Accepted: 6 August 2015 – Published: 27 August 2015

Correspondence to: A. Ito (akinorii@jamstec.go.jp)

Published by Copernicus Publications on behalf of the European Geosciences Union.

Title Page

Abstract

Introduction

Conclusions

References

Tables

Figures



Back

Close

Full Screen / Esc

Printer-friendly Version

Interactive Discussion



Fe supply to a significant portion of the oceans in the Northern Hemisphere, while their contribution to oceans in high latitudes remains uncertain due to limited understanding of dust Fe dissolution under pristine conditions.

1 Introduction

5 Changes in supply of nutrients such as bioavailable iron (Fe) from the atmosphere to the ocean have altered oceanic carbon uptake, but significant uncertainties remain on the magnitude of this effect (Ciais et al., 2013). Thus improved quantification of atmospheric delivery of bioavailable Fe is essential to estimate the long-term carbon sink more accurately (Jickells et al., 2005). The present study focuses on “potentially”
10 bioavailable Fe, which includes colloidal materials and aqueous species (often operationally defined as soluble Fe). The response of the aerosol Fe solubility (i.e., soluble Fe/total Fe) to air pollution is a key uncertainty in our understanding of the biogeochemical cycle of Fe, marine ecosystem, and climate (Mahowald et al., 2009; Shi et al., 2012; Hajima et al., 2014). We use the term “anthropogenic” soluble Fe here as
15 primary soluble Fe from oil combustion aerosols and secondary soluble Fe from both dust and combustion aerosols, due to the changes in emissions of precursor gases and aerosols from fossil fuel use and biofuel combustion between the preindustrial era and the present day (Ito et al., 2014).

20 Atmospheric processing of mineral dust has been hypothesized to be an important source of soluble Fe to the oceans because of acidic condition in aerosol water (Zhuang et al., 1992; Meskhidze et al., 2003). Previous chemical transport models used mineral dissolution rates and stoichiometric numbers of Fe in minerals to estimate Fe release rates from mineral aerosols (Meskhidze et al., 2005; Solmon et al., 2009; Ito and Feng, 2010; Ito, 2012). Laboratory studies for mineral dust have demonstrated that the Fe
25 release rates used in previous global models were much slower than the measurements during a typical aerosol lifetime of 2–7 days (Mackie et al., 2005; Shi et al., 2011). The initial period of enhanced concentration of elements, which are incongruently dis-

Anthropogenic bioavailable Fe deposition

A. Ito and Z. Shi

Title Page

Abstract

Introduction

Conclusions

References

Tables

Figures



Back

Close

Full Screen / Esc

Printer-friendly Version

Interactive Discussion



**Anthropogenic
bioavailable Fe
deposition**

A. Ito and Z. Shi

Title Page

Abstract

Introduction

Conclusions

References

Tables

Figures



Back

Close

Full Screen / Esc

Printer-friendly Version

Interactive Discussion



solved in solution from phyllosilicate minerals, is well known in laboratory works (e.g., Malmström and Banwart, 1997; Brandt et al., 2003). Much slower quasi-steady state dissolution rates after 10–14 days are typically observed for aluminosilicate minerals in acid solutions (Amram and Ganor, 2005; Lowson et al., 2005; Golubev et al., 2006; Rozalén et al., 2008; Bibi et al., 2011). Recent atmospheric chemical transport models have adopted the initial period of enhanced Fe release rate for the proton-promoted dissolution (Ito and Xu, 2014; Myriokefalitakis et al., 2015). It needs to be mentioned that the proton-promoted Fe dissolution is significantly suppressed due to the dust alkalinity, particularly in the Southern Hemisphere (Meskhidze et al., 2005; Ito and Feng, 2010; Johnson et al., 2010; Ito and Xu, 2014). Currently, ferric sulfate is treated as water-soluble Fe in oil combustion aerosols at emission (Ito, 2013, 2015; Myriokefalitakis et al., 2015; Wang et al., 2015).

Previous laboratory studies suggest that different acid types and photochemical reactions affect proton-promoted Fe dissolution rates of mineral dust in addition to the types of Fe species associated with mineral source materials (Cwiertny et al., 2008; Fu et al., 2010; Rubasinghege et al., 2010). However, all previous laboratory experiments were conducted in absence of ammonium salt, such as sulfate, which are ubiquitous in aerosol water. Some of anions in aerosol water are known to be effective inorganic ligands, which form the complexes with Fe in solution (Cornell and Schwertmann, 2003). In batch experiments, the mineral dissolution rate at high dust/liquid ratio can be influenced by different ability of these anions to form soluble complexes with metals (Hamer et al., 2003). Thus the effect of decrease of the activity of Fe^{3+} on the Fe dissolution rates via the formation of aqueous complexes needs to be assessed in laboratory experiments to constrain the degree of suppression used in models.

Recently, global atmospheric transport model studies have emphasized the role of oxalate for promoting Fe dissolution from Fe-containing aerosols (Luo and Gao, 2010; Johnson and Meskhidze, 2013; Ito, 2015; Myriokefalitakis et al., 2015) (see the Supplement). Moreover, oxalate-promoted dissolution of Fe is suppressed at low concentrations of oxalate near strong Fe sources (Ito, 2015), because excess oxalate is nec-

**Anthropogenic
bioavailable Fe
deposition**

A. Ito and Z. Shi

Title Page

Abstract

Introduction

Conclusions

References

Tables

Figures



Back

Close

Full Screen / Esc

Printer-friendly Version

Interactive Discussion



5 essary to induce significant Fe dissolution (Chen and Grassian, 2013). These model-
ing studies highlighted the importance of oxalate-promoted Fe dissolution for mineral
dust over the remote oceans. However, a constant oxalate-promoted dissolution rate
with time for mineral dust has been prescribed in previous models regardless of differ-
ent dissolution behaviors in different Fe types, due to a lack of experimental data for
oxalate-promoted Fe dissolution kinetics.

10 Here, we conducted a series of laboratory experiments to examine how inorganic
and organic ligands in solution (i.e., sulfate and oxalate) affect Fe dissolution rates
in mineral dust. The experimental data were then used to derive a new Fe release
scheme, which is implemented in a global chemical transport model to quantify the
effect of atmospheric processing of mineral aerosols on Fe mobilization. This study
incorporates the proton- and oxalate-promoted Fe dissolution schemes for the mineral
aerosols in our model (Ito, 2015). We also examine quasi-photo-reductive dissolution
scheme for mineral aerosols in a sensitivity simulation. Determination of Fe dissolu-
15 tion for different types of Fe requires three key parameters of Fe release rate, degree
of suppression, and Fe content. We implement three-stage kinetic process for the Fe
dissolution scheme to dust aerosols. We use the updated version of the mineralogical
database for Fe content in soils (Journet et al., 2014). To assess model assumptions
for Fe dissolution, the calculated Fe solubility is evaluated against field observations in
20 relation to total Fe loading and water soluble organic carbon (WSOC) over the North
Atlantic Ocean (Wozniak et al., 2013, 2015). The model provides the soluble Fe supply
from both dust and combustion sources to the oceans in association with past changes
in air quality based on the Intergovernmental Panel on Climate Change (IPCC) emis-
sion data set. The experimental and model approaches are presented in Sects. 2 and
3, respectively. Section 4 describes the experimental results and the development of
25 the new Fe release scheme. The response of soluble Fe deposition to changes in air
pollution and the comparisons of the model with observations are described in the
Sect. 5 followed by the summary of our findings in the Sect. 6.

2 Laboratory experiments

In this study, we used the same Tibesti dust sample as in Shi et al. (2011, 2015). We followed a similar methodology as in Shi et al. (2011). Please see Supplement for more details. Highly reactive Fe on the mineral surface was 0.63% of the total Fe (Shi et al., 2011). More crystalline Fe oxides on the mineral surface represent 37.7% of total Fe in the Tibesti dust. The rest of Fe is associated with aluminosilicates.

In order to determine the Fe dissolution kinetics in the dust aerosol water, which contains organic ligands, such as oxalate, and high concentration of inorganic ions, such as sulfate, four sets of time dependent dissolution experiments were performed following the same methodology as in Shi et al. (2011). The experiments include the dissolution of Fe in the Tibesti dust:

(Experiment 1) at a dust/liquid ratio of 1 g L^{-1} in 0.05 and 0.005 mol L^{-1} sulfuric acid solution only (i.e., no $(\text{NH}_4)_2\text{SO}_4$) ($\text{pH} = 1.3$, ionic strength $I = 0.15 \text{ M}$; and $\text{pH} = 2.1$, $I = 0.015 \text{ M}$). The pH values in highly acidic solutions were estimated from molality and activity coefficient, which were calculated using E-AIM III aqueous solution simulator (Wexler and Clegg, 2002).

(Experiment 2) at a dust/liquid ratio of 1 g L^{-1} in 0.05 and $0.0005 \text{ mol L}^{-1}$ sulfuric acid solution with 1 mol L^{-1} $(\text{NH}_4)_2\text{SO}_4$ ($\text{pH} = 2$ and $I = 3.15 \text{ M}$; and $\text{pH} = 3.1$ and $I = 3.015 \text{ M}$) only (i.e., no oxalate) and in 0.1 mol L^{-1} HCl solution with 3 mol L^{-1} NH_4Cl (ionic strength $I = 3.2 \text{ mol L}^{-1}$) ($\text{pH} = 0.9$; note that activity coefficient for H^+ in this solution is higher than 1), and at a dust/liquid ratio of 10 g L^{-1} in 0.05 mol L^{-1} sulfuric acid solution with 1 mol L^{-1} $(\text{NH}_4)_2\text{SO}_4$ ($\text{pH} = 2$, $I = 3.15 \text{ mol kg}^{-1}$). The pH values with high ionic strength ($I > 3 \text{ mol L}^{-1}$) were estimated using E-AIM III thermodynamic model (Wexler and Clegg, 2002).

(Experiment 3) at a dust/liquid ratio of 1 g L^{-1} in 0.05 and $0.0005 \text{ mol L}^{-1}$ sulfuric acid solution with both 1 mol L^{-1} $(\text{NH}_4)_2\text{SO}_4$ and 0.03 mol L^{-1} of oxalate (as sodium oxalate) ($\text{pH} = 2$, $I = 3.15 \text{ M}$; and $\text{pH} = 3.1$, $I = 3.015 \text{ M}$). The chosen amount of oxalate is based on the molar ratio of oxalate and sulfate in ambient $\text{PM}_{2.5}$ samples (Yu et al., 2005).

Anthropogenic bioavailable Fe deposition

A. Ito and Z. Shi

Title Page

Abstract

Introduction

Conclusions

References

Tables

Figures



Back

Close

Full Screen / Esc

Printer-friendly Version

Interactive Discussion



**Anthropogenic
bioavailable Fe
deposition**

A. Ito and Z. Shi

Title Page

Abstract

Introduction

Conclusions

References

Tables

Figures



Back

Close

Full Screen / Esc

Printer-friendly Version

Interactive Discussion



(Experiment 4) at a dust/liquid ratio of 60 mg L^{-1} , 10 and 50 g L^{-1} in 0.005 mol L^{-1} sulfuric acid solution (pH 2). The pH was continuously monitored during the experiments at four different dust/liquid ratios (i.e., 60 mg L^{-1} , 1 , 10 and 50 g L^{-1}) and once the pH change was more than 0.1 pH unit, acids were added to decrease the pH to 2. This aims to determine how different dust/liquid ratios affect the Fe dissolution kinetics in comparison with Experiment 1 (1 g L^{-1}).

At each chosen time point, an aliquot of the dust suspension was taken with a syringe and filtered through a $0.2 \mu\text{m}$ filter directly into HCl (final concentration 0.2 N HCl), and the filtrates were stored for a maximum of one month at 4°C until Fe analysis. Filtration through $0.2 \mu\text{m}$ pore sized filters is commonly used for measurements of dissolved species from dust suspension, especially at near-neutral pH. Fe colloids tend to aggregate or adhere to mineral surface, which are efficiently retained by a $0.2 \mu\text{m}$ filter (Shi et al., 2009, 2015). Spectrophotometric ferrozine method was used to quantify the dissolved Fe concentration in this study. The solutions from the high ionic experiments ($I > 3 \text{ mol L}^{-1}$) were diluted 100 times with acidified Milli-Q water (0.01 mol L^{-1} HCl) before measurement to avoid interferences. The precision of Fe measurement is $\pm 1.2\%$ (1 s , $n = 6$) and the detection limit for dissolved Fe is $0.05 \mu\text{M}$ (Shi et al., 2015).

3 Model description

This study uses the Integrated Massively Parallel Atmospheric Chemical Transport (IMPACT) model (Rotman et al., 2004; Liu et al., 2005; Feng and Penner, 2007; Ito et al., 2007, 2012, 2014, 2015; Lin et al., 2014; Xu and Penner, 2012; Ito, 2015). The model is driven by assimilated meteorological fields from the Goddard Earth Observation System (GEOS) of the NASA Global Modeling and Assimilation Office (GMAO). Simulations have been performed with a horizontal resolution of $2.0^\circ \times 2.5^\circ$ and 59 vertical layers using meteorological fields for the years 2010 (and 2011 for the comparison with the field measurements).

4 Development of a new Fe dissolution scheme based on new experimental results

In our model, Fe release from aerosols due to chemical processing is calculated based on an online simulation of aqueous-phase chemistry (Ito and Feng, 2010; Ito, 2012, 2015; Ito and Xu, 2014). Ito and Xu (2014) have developed a Fe dissolution scheme that considers the types of Fe species associated with mineral source materials, mainly based on the measurements by Shi et al. (2011). Following their studies, three Fe pools are characterized by ferrihydrite, nano-sized Fe oxides, and heterogeneous inclusion of nano-Fe grains in aluminosilicates (e.g., illite, smectite, and chlorite). Here we developed a new Fe dissolution scheme, which considers our laboratory experimental datasets regarding: (1) the formation of Fe inorganic and organic complexes in solution and (2) the formation of surface complexes between oxalate and Fe oxides, following Ito (2015) for combustion aerosols.

Figure 1 and Fig. S1 in the Supplement demonstrate the effects of inorganic anions to form soluble complexes with Fe at different dust/liquid ratios on dissolution rates measured in acidic solution. Figure 1 shows that the pH = 2 (0.05 M H₂SO₄, 1 M (NH₄)₂SO₄, red triangles) and pH = 2.1 (0.005 M H₂SO₄, green diamonds) cases at 1 g L⁻¹ have significantly different Fe dissolution rates. The one with high ionic strength has a much higher dissolution rate than predicted by the small difference in the pH values. It is expected that one pH unit can lead to 3–4 times difference in dissolution rates as shown here and by Shi et al. (2011). Higher ionic strength has a tendency to decrease the thermodynamic solubility but the presence of complexing ions such as sulfate in this case has the potential to accelerate the dissolution rate by absorption or by complexation with Fe dissolved in solution (Cornell and Schwertmann, 2003). We observed a good agreement of measurements between at 1 g L⁻¹ dust in 0.05 mol L⁻¹ sulfuric acid solution with 1 mol L⁻¹ (NH₄)₂SO₄ (pH = 2.0, red triangles) and at 60 mg L⁻¹ dust in 0.005 mol L⁻¹ sulfuric acid solution without (NH₄)₂SO₄ (pH = 2.11, black circles). Thus the solution remains under-saturated with respect to Fe(III), because es-

Anthropogenic bioavailable Fe deposition

A. Ito and Z. Shi

[Title Page](#)[Abstract](#)[Introduction](#)[Conclusions](#)[References](#)[Tables](#)[Figures](#)[Back](#)[Close](#)[Full Screen / Esc](#)[Printer-friendly Version](#)[Interactive Discussion](#)

5 sentially all aqueous Fe(III) species (> 99%) is complexed with sulfate (i.e., FeSO_4^+) in 0.05 mol L^{-1} sulfuric acid solution with 1 mol L^{-1} $(\text{NH}_4)_2\text{SO}_4$ (pH = 2.0) (Meskhidze et al., 2005; Ito, 2015). The higher dust/liquid ratio at 10 g L^{-1} (blue squares) exhibits lower Fe dissolution rate after the initial period of enhanced Fe release rate, possibly
10 due to the re-adsorption of solution phase Fe onto the particulate phase, as the solution with $(\text{NH}_4)_2\text{SO}_4$ is under-saturated with respect to Fe(III) (Spokes and Jickells, 1996; Bibi et al., 2011).

Our data indicate that addition of complexing agents (i.e., sulfate in Fig. 1 and chlorite in Fig. S1 in the Supplement) accelerated dissolution of Fe minerals by binding
15 Fe released from the surface in solution (Zhang et al., 1985; Xu and Gao, 2008). Almost identical slopes were found between at 1 g L^{-1} dust in 0.05 mol L^{-1} sulfuric acid solution with 1 mol L^{-1} $(\text{NH}_4)_2\text{SO}_4$ (pH = 2.0, red triangles) and at 60 mg L^{-1} dust in 0.005 mol L^{-1} sulfuric acid solution without $(\text{NH}_4)_2\text{SO}_4$ (pH = 2.0, black circles) during a typical aerosol lifetime (Fig. 1). Thus we chose dust/liquid ratios of 1 g L^{-1} in sulfuric acid solution with 1 M ammonium sulfate to represent proton-promoted Fe dissolution scheme for mineral dust.

Figure 2 demonstrates the impact of oxalate on Fe dissolution rate (black circles). The addition of $0.03 \text{ M Na}_2\text{C}_2\text{O}_4$ accelerated the dissolution of Fe in dust (1 g dust L^{-1} solution, $0.05 \text{ M H}_2\text{SO}_4$ or $0.005 \text{ M H}_2\text{SO}_4$, with $1 \text{ M } (\text{NH}_4)_2\text{SO}_4$). Dissolved Fe concentration was 60% higher at 72 h in the $0.05 \text{ M H}_2\text{SO}_4$ and $1 \text{ M } (\text{NH}_4)_2\text{SO}_4$ dust suspensions with oxalate. It was over 100% higher at 72 h in the $0.005 \text{ M H}_2\text{SO}_4$ and $1 \text{ M } (\text{NH}_4)_2\text{SO}_4$ dust suspensions when added oxalate. The higher activity of protons can facilitate the oxalate-promoted dissolution process by protonating the hydroxyl (OH) groups at the surface of hydrous Fe oxides, thereby contributing to increasing the number of positively charged surface sites. This increase promotes ligand adsorption, and weakening of the Fe-O bond, which permits the reaction between oxalate and Fe sites by ligand exchange (Cornell and Schwertman, 2003; Ramos et al., 2014). Although the protonation of the ligands in solution increases at higher activity of protons, the adsorption mechanism of HC_2O_4^- involves the loss of a proton during the ligand-exchange
25

Anthropogenic bioavailable Fe deposition

A. Ito and Z. Shi

Title Page

Abstract

Introduction

Conclusions

References

Tables

Figures



Back

Close

Full Screen / Esc

Printer-friendly Version

Interactive Discussion



Anthropogenic bioavailable Fe deposition

A. Ito and Z. Shi

Title Page

Abstract

Introduction

Conclusions

References

Tables

Figures



Back

Close

Full Screen / Esc

Printer-friendly Version

Interactive Discussion



adsorption reaction or during the transfer process from bulk solution to the mineral surface (Yoon et al., 2004). Consequently, the amount of absorbed complex on the mineral surface is higher in solutions at $\text{pH} < 7$ when the overall charge at the reactive surface sites is positive, compared to that at lower activity of protons (Zhang et al., 1985; Xu and Gao, 2008; Lanzl et al., 2012; Ramos et al., 2014). The surface binding sites for adsorbed oxalate become saturated at high proton and high oxalate concentrations, and thus oxalate-promoted dissolution rates are almost independent of pH for mineral dust (Yoon et al., 2004; Cama and Ganor, 2006; Lanzl et al., 2012).

Experimental data in Fig. 3 demonstrate that the Fe release under higher dust/solution ratios is suppressed when the solution becomes super-saturated with respect to Fe(III), as observed by the decrease in the rate (black circles). At low dust/liquid ratio of 60 mg L^{-1} at pH 2.1 (H^+ concentration of 0.01 mol L^{-1}), Fe dissolution continued even after 800 h. The rate of Fe dissolution decreased substantially with increasing dust/liquid ratio. At a dust/liquid ratio of 50 g L^{-1} , Fe dissolution stopped at 180 h and only 1.2% ($10 \text{ } \mu\text{mol g}^{-1}$) of the total Fe was dissolved, half of which released in the first hour. According to Shi et al. (2011), this corresponds to the first Fe pool of Tibesti- PM_{20} at $\text{pH} = 2$. The calculated thermodynamic solubility of this Fe pool at pH 2 is -3.34 (mol L^{-1} on a log scale). This is slightly larger than the measured thermodynamic solubility of nanogoethite, which is -3.6 (mol L^{-1}) at $\text{pH} = 2$ (see Fig. 7 in Shi et al., 2011). This Fe pool can include ferrihydrite and reactive nano-Fe oxides aggregated on the mineral surface. This is also consistent with higher Fe solubility of 1.2% than highly reactive Fe (0.63%) (Shi et al., 2011). Only 3.3% of Fe was dissolved at a dust/liquid ratio of 10 g L^{-1} and pH 2, and Fe dissolution stopped at 180 h. According to Shi et al. (2011), this represents the total of first and second Fe pools of Tibesti- PM_{20} at $\text{pH} = 2$. The calculated thermodynamic solubility of the second Fe pool is -3.55 (mol L^{-1}). The above experimental dataset is used to determine the model parameters to predict the influence of solution saturation state on the Fe dissolution rates (see discussion on Fig. 3 below).

Anthropogenic bioavailable Fe deposition

A. Ito and Z. Shi

Title Page

Abstract

Introduction

Conclusions

References

Tables

Figures



Back

Close

Full Screen / Esc

Printer-friendly Version

Interactive Discussion



Based on above laboratory results (Figs. 2 and 3), Fe dissolution from mineral dust aerosols is treated explicitly as a kinetic process that depends on the pH, ambient temperature, the degree of solution saturation, and competition for oxalate between surface Fe and dissolved Fe in our model (Table 2). The net Fe dissolution rates (ΣR_{Fe_i} , in units of moles of dissolved Fe per Fe gram of Fe-containing mineral particle per second) for the proton-promoted ($i = 1$), oxalate-promoted ($i = 2$), and quasi-photo-reductive ($i = 3$) Fe dissolution schemes can be empirically described using the following equation, which is similar to the formulation applied for Fe-containing minerals (Zhang et al., 1985; Lasaga et al., 1994; Hamer et al., 2003; Meskhidze et al., 2005; Lanzl et al., 2012; Ito and Xu, 2014; Ito, 2015):

$$R_{\text{Fe}_i} = k_i(\text{pH}, T) \times a(\text{H}^+)^{m_i} \times f_i \times g_i \quad (1)$$

where k_i is the “far-from-equilibrium” (i.e., $f_i = 1$ and $g_i = 1$) Fe release rate (moles Fe $\text{g}^{-1} \text{s}^{-1}$), $a(\text{H}^+)$ is the H^+ activity, m_i represents the empirical reaction order for protons, and f_i and g_i account for the suppression.

The Fe release rate, k_i , is estimated for the proton- and oxalate-promoted dissolution schemes by fitting the parameters to our measurements in sulfuric acid and ammonium sulfate (Experiment 2 and 3) with and without oxalate (Fig. 2). Fe release from mineral dust under acidic conditions is characterized by initial rapid Fe release and subsequent slow Fe release (Desboeufs et al., 1999; Mackie et al., 2005; Cwiertny et al., 2008; Shi et al., 2011). Since the typical lifetime of mineral dust is about a week, the initial rapid Fe release rates are important for the atmospheric processing of mineral dust. The three-stage kinetic model is used to describe the Fe release behavior of mineral dust: 1st stage is characterized by a rapid dissolution of hydrous ferric oxide (HFO) on the surface of minerals, 2nd stage is an intermediate stage of nano-sized Fe oxides dissolution from the surface of minerals, and 3rd stage is the Fe release from fine-grained materials, which are internally mixed with aluminosilicate particles, as the mineral surface is slowly dissolved. Here, we prescribe the content of HFO (0.65 %) and nano-sized Fe oxides (1.3 %) on the surface of minerals. The content of HFO is consistent

at higher pH values, no pH effect on the quasi-photo-induced Fe dissolution for mineral aerosols was performed in the sensitivity simulation. In analogy to the combustion aerosols (Chen and Grassian, 2013; Ito, 2015), we apply the same rate constant to quasi-photo-induced dissolution as in oxalate-promoted dissolution and we set $f_3 = 1$ in Eq. (1). The quasi-photo-induced dissolution rate is calculated by scaling the photolysis rate of H_2O_2 estimated in the model, following Ito (2015). The photo-degradation of oxalate due to photolysis of Fe-oxalate complexes is simulated for Fe-containing aerosols in aqueous chemistry (Lin et al., 2014; Ito, 2015).

5 Modeling results and discussion

The model-calculated concentrations of total and soluble Fe in aerosols have been extensively compared with field observations (Ito and Feng, 2010; Ito, 2012, 2013, 2015; Ito and Xu, 2014). Here, model-calculated daily average surface concentrations of soluble Fe (red squares) were compared with the measurements (black circles) during the 2010 and 2011 US GEOTRACES cruise over the North Atlantic (Fig. 4) (Wozniak et al., 2013, 2015). The model-calculated variability at each latitude and longitude represents the daily variability during the sampling dates. The modeled soluble Fe concentration exhibits a latitudinal variability, which is similar to that of the measurements, with low values over the remote ocean ($< 0.5 \text{ ng m}^{-3}$), intermediate values near European continents, and high values near North African continents ($> 5 \text{ ng m}^{-3}$) (Fig. 4a). The modeled soluble Fe concentration shows a longitudinal variability, which is also similar to that of the measurements, with low values over the remote ocean ($< 0.5 \text{ ng m}^{-3}$), intermediate values near North American continents, and high values near North African continents ($> 2 \text{ ng m}^{-3}$) (Fig. 4b).

Figure 5 displayed the daily averaged, model-calculated surface total aerosol Fe loading, Fe solubility, Fe/WSOC molar ratio, and dust/combustion ratio for soluble Fe (red squares) over the 2010 and 2011 US GEOTRACES cruise tracks in comparison with the measurements (black circles) by Wozniak et al. (2013, 2015). As previously re-

Anthropogenic bioavailable Fe deposition

A. Ito and Z. Shi

[Title Page](#)[Abstract](#)[Introduction](#)[Conclusions](#)[References](#)[Tables](#)[Figures](#)[Back](#)[Close](#)[Full Screen / Esc](#)[Printer-friendly Version](#)[Interactive Discussion](#)

**Anthropogenic
bioavailable Fe
deposition**

A. Ito and Z. Shi

Title Page

Abstract

Introduction

Conclusions

References

Tables

Figures



Back

Close

Full Screen / Esc

Printer-friendly Version

Interactive Discussion



ported in Ito (2013), the oil combustion from shipping mainly contributes to high Fe solubility at low Fe loading observed over the high latitude North Atlantic Ocean (Fig. 5a). In this study, low Fe solubility near North African continent was successfully simulated. While our model has incorporated the initial rapid Fe release rate in acid solutions with oxalate explicitly, the comparisons with observations support the suppression of Fe dissolution under low acidity and low oxalate concentration near the source region of dust aerosols. Furthermore, the Fe/WSOC molar ratios in aerosols influenced by combustion aerosols are 2–3 orders of magnitude lower than those near North African continent, which are also consistent with the observations (Wozniak et al., 2013, 2015) (Fig. 5b). The use of our process-based model demonstrates that chemical reactions and mixing with combustion aerosols are the main mechanisms to cause the high Fe solubility at low Fe loading in the North Atlantic (Fig. 5c). As previously discussed in Ito (2013), this is consistent with the observations (e.g., Sedwick et al., 2007; Séguret et al., 2011).

The suppression of Fe dissolution under low proton and low oxalate concentrations leads to the lower Fe solubility of mineral dust deposited to the ocean (0.64–0.71 %) on a global mean in present days (Table 4). The Fe solubility for mineral dust varies spatially over the remote oceans, due to the proton-, oxalate-promoted, and quasi-photo-reductive Fe dissolution (Fig. 6). The Fe solubility ranges from 0.75 to 2 % over the North Atlantic and Pacific in present days (Fig. 6a and c), which is relatively consistent with that (1–2 %) used in conventional ocean biogeochemical models (Jickells et al., 2005). The base simulations result in low Fe solubility ($< 1\%$) over the Southern Ocean in present days and significant portions of the ocean in preindustrial era, due to the suppression of Fe dissolution under low proton concentrations (Fig. 6a and b). In contrast, the sensitivity simulations for mineral aerosols (i.e., $f_3 = 1$) lead to higher Fe solubility ($> 1\%$) deposited to the remote oceans of high nitrate, low chlorophyll (HNLC) regions such as the subarctic north Pacific, the east equatorial Pacific, and the Southern Ocean, when quasi-photo-reductive dissolution was considered at higher pH values (Fig. 6c and d).

**Anthropogenic
bioavailable Fe
deposition**

A. Ito and Z. Shi

Title Page

Abstract

Introduction

Conclusions

References

Tables

Figures



Back

Close

Full Screen / Esc

Printer-friendly Version

Interactive Discussion



The annually averaged rate of deposition of soluble Fe from dust and combustion sources to the oceans is presented in Fig. 7a and d for the base and sensitivity simulations, respectively. The total Fe solubility (Fig. 7b and e) is higher than that calculated from dust only over significant portions of the open ocean. However, our modeled Fe solubility (0.1–0.5 and 0.2–0.7 % for the base and sensitivity simulations, respectively) is still low over the South Atlantic east downwind from the Patagonian dust source regions where previous modeled Fe solubility deposited to the ocean (1.4–2.0 % by Mahowald et al., 2009; 0.5–0.6 % by Johnson et al., 2010) was significantly lower than that deduced from observations (7.5–20 % by Baker et al., 2013). Our modeled Fe solubility for dry deposition over the Atlantic (1.1 ± 1.9 and 1.2 ± 2.0 %) is in good agreement the measurement (2.1 ± 2.2 %), while that for wet deposition (3.4 ± 3.2 and 3.6 ± 3.3 %) is significantly lower than the measurement (10.4 ± 4.6 %) (Baker et al., 2013). Moreover, our monthly averaged Fe solubility (1–4 %) in wet deposition is an order of magnitude lower than that observed on the Kerguelen Islands in South Indian Ocean (82 ± 18 % by Heimburger et al., 2013). This enhanced solubility may be due to unidentified reactive organic species in cloud water, which contain Fe-binding functionalities (e.g., $-\text{COOH}$, $-\text{NH}_2$) such as humic-like substances from biomass burning and biologically derived materials from the ocean (Parazols et al., 2006; Deguillaume et al., 2014; Ito et al., 2014, 2015). The role of humic-like substances in the complexation and dissolution of Fe oxides over a wide pH range has received considerable attention in recent literatures (Al-Abadleh, 2015). The multiple ligands with high affinity for Fe binding can wrest aqueous Fe from any Fe–oxalate complexes, allow the oxalate ligand to react with the surface Fe oxides, and assist the Fe–oxalate detachment from the surface Fe oxides at intermediate pH (e.g., pH = 5) (Cheah et al., 2003). On the other hand, functional groups on the humic molecule are less protonated at pH > 4, increase the probability of coating of organic matters on the reactive mineral surfaces, and thus inhibit the oxalate-promoted dissolution (Drever and Stillings, 1997). Clearly, more work is required to elucidate the underlying mechanisms that promote Fe dissolution in cloud water over the Southern Ocean in future studies.

Anthropogenic bioavailable Fe deposition

A. Ito and Z. Shi

Title Page

Abstract

Introduction

Conclusions

References

Tables

Figures



Back

Close

Full Screen / Esc

Printer-friendly Version

Interactive Discussion



The contributions of anthropogenic soluble Fe deposition to the present-days are examined in Fig. 7c and f for the base and sensitivity simulations, respectively. The soluble Fe deposition from both mineral dust and fossil fuel combustion sources due to changes in atmospheric pollution contributes more than half of the total soluble Fe deposition over significant portions of the open ocean in the Northern Hemisphere for the base simulations. The sensitivity simulations for mineral aerosols (i.e., $f_3 = 1$) lead to higher soluble Fe deposition in both present days preindustrial era (Table 3) and result in lower anthropogenic soluble Fe deposition to the HNLC regions, due to almost no pH dependency of the quasi-photo-reductive dissolution. Of the total soluble Fe deposition from anthropogenic sources (excluding biomass burning) to the ocean (0.05–0.06 Tg Fe yr⁻¹), 67–72 % is from dust sources, 28–33 % is from fossil fuel combustion (Table 3). In contrast, our model indicated higher contribution of biomass burning aerosols in preindustrial era (42–55 % in total soluble Fe deposition to the ocean). It should be noted, however, significant uncertainties remain on the magnitude of this source strength (Luo et al., 2008; Ito, 2011, 2012, 2015; Wang et al., 2015).

Our estimate of total Fe deposition to the ocean (10 Tg Fe yr⁻¹) is within the range of other models (Table 4). Our estimates of soluble Fe deposition to the oceans (0.05 and 0.07 Tg Fe yr⁻¹ from the base and sensitivity simulations, respectively) in preindustrial era are in good agreement with that of Myriokefalitakis et al. (2015) (Table 4). The ratio of present-day soluble Fe deposition to the preindustrial era from the base simulation (47 %) is in good agreement with that estimated by Luo et al. (2008) (46 %), despite the use of various dissolution schemes, emission data sets, and atmospheric transport models. The sensitivity simulations, which include the quasi-photo-reductive dissolution for mineral aerosols (i.e., $f_3 = 1$), results in relatively small increases in the soluble Fe deposition in the global ocean (0.077 and 0.122 Tg Fe yr⁻¹ on a global mean in preindustrial and present days, respectively). The global deposition is similar between our two simulations, mainly because of the suppression of proton-promoted (i.e., f_1) and oxalate-promoted (i.e., g_2) dissolution near the strong source regions of mineral dust. This is reflected in lower Fe solubility (1.1–1.2 % on a global mean), compared to

those estimated by previous modeling studies (1.4–15 %, see Table 5 in Hajima et al., 2014).

6 Conclusions

We have developed a new scheme of Fe dissolution, which reproduced the proton- and oxalate-promoted dissolution behaviors of our experimental results for mineral dust. The batch dissolution experiments provided the Fe dissolution rates under far from equilibrium conditions and the parameters for degree of suppression as the saturation state approached equilibrium. To investigate the uncertainty in the Fe dissolution associated with organic compounds, negligible pH effect on the quasi-photo-induced Fe dissolution for mineral aerosols was performed in the sensitivity simulations. The Fe release scheme allows us to reduce the number of mineral tracers for implementation in the Earth system models. At lower proton activity and lower oxalate concentration in aerosol water on dust particles near major dust sources, both proton and oxalate had no significant effect on the Fe dissolution in our model. Fe release under more acidic condition in aerosol water due to air pollution resulted in significant increases in soluble Fe deposition over large portions of the open ocean in the Northern Hemisphere. In our model, low Fe solubility is estimated for mineral dust ($< 1\%$) over the Southern Ocean downwind from the dust source regions. The differences between our base and sensitivity simulations for mineral aerosols are notable for low Fe loading over the remote HNLC regions such as the subarctic north Pacific, the east equatorial Pacific, and the Southern Ocean. However, the differences in Fe solubility between different simulations are generally smaller than the differences between different model estimates and measurements. A comprehensive comparison of model predicted Fe and its related species with observations is therefore needed to elucidate the high Fe solubility observed under pristine conditions.

Anthropogenic bioavailable Fe deposition

A. Ito and Z. Shi

Title Page

Abstract

Introduction

Conclusions

References

Tables

Figures



Back

Close

Full Screen / Esc

Printer-friendly Version

Interactive Discussion



Acknowledgements. Support for this research was provided to A. Ito by Program for Risk Information on Climate Change (MEXT). All of the numerical simulations were performed using the SGI ICE X at the JAMSTEC. Z. Shi is supported by UK Natural Environment Research Council (NE/I021616/1, NE/K000845/1) and the Royal Society. We would like to thank E. Journet and Y. Balkanski for making the mineralogical database available. We are grateful to R. Shelley, L. William, and their colleagues for kindly providing the observational data set during the 2010 US GEOTRACES cruise, supported by NSF, USA, OCE-0752832, 0929919, and 1132766.

References

- Al-Abadleh, H. A.: Review of the bulk and surface chemistry of iron in atmospherically relevant systems containing humic-like substances (HULIS), RSC Adv., 5, 45785–45811, doi:10.1039/c5ra03132j, 2015.
- Amram, K. and Ganor, J.: The combined effect of pH and temperature on smectite dissolution rate under acidic conditions, Geochim. Cosmochim. Ac., 69, 2535–2546, doi:10.1016/j.gca.2004.10.001, 2005.
- Baker, A. R., Adams, C., Bell, T. G, Jickells, T. D., and Ganzeveld, L.: Estimation of atmospheric nutrient inputs to the Atlantic Ocean from 50° N to 50° S based on large-scale field sampling: iron and other dust-associated elements, Global Biogeochem. Cy., 27, 755–767, doi:10.1002/gbc.20062, 2013.
- Bibi, I., Singh, B., and Silvester, E.: Dissolution of illite in saline–acidic solutions at 25 °C, Geochim. Cosmochim. Ac., 75, 3237–3249, doi:10.1016/j.gca.2011.03.022, 2011.
- Bibi, I., Singh, B., and Silvester, E.: Dissolution kinetics of soil clays in sulfuric acid solutions: ionic strength and temperature effects, Appl. Geochem., 51, 170–183, doi:10.1016/j.apgeochem.2014.10.004, 2014.
- Bonneville, S., Van Cappellen, P., and Behrends, T.: Microbial reduction of iron(III) oxyhydroxides: effects of mineral solubility and availability, Chem. Geol., 212, 255–268, doi:10.1016/j.chemgeo.2004.08.015, 2004.

**Anthropogenic
bioavailable Fe
deposition**

A. Ito and Z. Shi

Title Page

Abstract

Introduction

Conclusions

References

Tables

Figures



Back

Close

Full Screen / Esc

Printer-friendly Version

Interactive Discussion



- Brandt, F., Bosbach, D., Krawczyk-Bärsch, E., Arnold, T., and Bernhard, G.: Chlorite dissolution in the acid pH-range: a combined microscopic and macroscopic approach, *Geochim. Cosmochim. Ac.*, 67, 1451–1461, doi:10.1016/S0016-7037(02)01293-0, 2003.
- 5 Cama, J. and Ganor, J.: The effects of organic acids on the dissolution of silicate minerals: a case study of oxalate catalysis of kaolinite dissolution, *Geochim. Cosmochim. Ac.*, 70, 2191–2209, doi:10.1016/j.gca.2006.01.028, 2006.
- Ciais, P., Sabine, C., Govindasamy, B., Bopp, L., Brovkin, V., Canadell, J., Chhabra, A., DeFries, R., Galloway, J., Heimann, M., Jones, C., Le Quéré, C., Myneni, R., Piao, S., and Thornton, P.: Carbon and other biogeochemical cycles, chapt. 6, in: *Climate Change 2013 The Physical Science Basis*, edited by: Stocker, T., Qin, D., and Plattner, G.-K., Cambridge University Press, Cambridge, 465–570, 2013.
- 10 Cheah, S. F., Kraemer, S. M., Cervini-Silva, J., and Sposito, G.: Steady-state dissolution kinetics of goethite in the presence of desferrioxamine B and oxalate ligands: implications for the microbial acquisition of iron, *Chem. Geol.*, 198, 63–75 doi:10.1016/S0009-2541(02)00421-7, 2003.
- 15 Chen, H. and Grassian, V. H.: Iron dissolution of dust source materials during simulated acidic processing: the effect of sulfuric, acetic, and oxalic acids, *Environ. Sci. Technol.*, 47, 10312–10321, doi:10.1021/es401285s, 2013.
- Cornell, R. M. and Schwertmann, U.: *The Iron Oxides: Structure, Properties, Reactions, Occurrence and Uses*, Wiley-VCH Publishers, New York, 2003.
- 20 Cwiertny, D. M., Baltrusaitis, J., Hunter, G. J., Laskin, A., Scherer, M. M., and Grassian, V. H.: Characterization and acid-mobilization study of iron-containing mineral dust source materials, *J. Geophys. Res.*, 113, D05202, doi:10.1029/2007jd009332, 2008.
- Deguillaume, L., Desboeufs, K. V., Leriche, M., Long, Y., and Chaumerliac, N.: Effect of iron dissolution on cloud chemistry: from laboratory measurements to model results, *Atmos. Pollut. Res.*, 1, 220–228, doi:10.5094/APR.2010.029, 2010.
- 25 Deguillaume, L., Charbouillot, T., Joly, M., Vaïtilingom, M., Parazols, M., Marinoni, A., Amato, P., Delort, A.-M., Vinatier, V., Flossmann, A., Chaumerliac, N., Pichon, J. M., Houdier, S., Laj, P., Sellegri, K., Colomb, A., Brigante, M., and Mailhot, G.: Classification of clouds sampled at the puy de Dôme (France) based on 10 yr of monitoring of their physicochemical properties, *Atmos. Chem. Phys.*, 14, 1485–1506, doi:10.5194/acp-14-1485-2014, 2014.
- 30 Desboeufs, K., Losno, R., Vimeux, F., and Cholbi, S.: pH dependent dissolution of wind transported Saharan dust, *J. Geophys. Res.*, 104, 21287–21299, 1999.

**Anthropogenic
bioavailable Fe
deposition**

A. Ito and Z. Shi

Title Page

Abstract

Introduction

Conclusions

References

Tables

Figures



Back

Close

Full Screen / Esc

Printer-friendly Version

Interactive Discussion



- Drever, J. I. and Stillings, L. L.: The role of organic acids in mineral weathering, *Colloids Surfaces A*, 120, 167–181, 1997.
- Feng, Y. and Penner, J. E.: Global modeling of nitrate and ammonium: interaction of aerosols and tropospheric chemistry, *J. Geophys. Res.*, 112, D01304, doi:10.1029/2005JD006404, 2007.
- 5 Golubev, S. V., Bauer, A., and Pokrovsky, O. S.: Effect of pH and organic ligands on the kinetics of smectite dissolution at 25°C, *Geochim. Cosmochim. Ac.*, 70, 4436–4451, doi:10.1016/j.gca.2006.06.1557, 2006.
- Hajima, T., Kawamiya, M., Watanabe, M., Kato, E., Tachiiri, K., Sugiyama, M., Watanabe, S., Okajima, H., and Ito, A.: Modeling in Earth system science up to and beyond IPCC AR5, *Progress in Earth and Planetary Science*, 1, 1–25, doi:10.1186/s40645-014-0029-y, 2014.
- 10 Hamer, M., Graham, R., Amrhein, C., and Bozhilov, K.: Dissolution of ripidolite (Mg, Fe-chlorite) in organic and inorganic acid solutions, *Soil Sci. Soc. Am. J.*, 67, 654–661, 2003.
- Heimburger, A., Losno, R., and Triquet, S.: Solubility of iron and other trace elements in rain-water collected on the Kerguelen Islands (South Indian Ocean), *Biogeosciences*, 10, 6617–6628, doi:10.5194/bg-10-6617-2013, 2013.
- 15 Ito, A.: Mega fire emissions in Siberia: potential supply of bioavailable iron from forests to the ocean, *Biogeosciences*, 8, 1679–1697, doi:10.5194/bg-8-1679-2011, 2011.
- Ito, A.: Contrasting the effect of iron mobilization on soluble iron deposition to the ocean in the Northern and Southern Hemispheres, *J. Meteorol. Soc. Jpn.*, 90A, 167–188, doi:10.2151/jmsj.2012-A09, 2012.
- 20 Ito, A.: Global modeling study of potentially bioavailable iron input from shipboard aerosol sources to the ocean, *Global Biogeochem. Cy.*, 27, 1–10, doi:10.1029/2012GB004378, 2013.
- 25 Ito, A.: Atmospheric processing of combustion aerosols as a source of bioavailable iron, *Environ. Sci. Technol. Lett.*, 2, 70–75, doi:10.1021/acs.estlett.5b00007, 2015.
- Ito, A. and Feng, Y.: Role of dust alkalinity in acid mobilization of iron, *Atmos. Chem. Phys.*, 10, 9237–9250, doi:10.5194/acp-10-9237-2010, 2010.
- 30 Ito, A. and Xu, L.: Response of acid mobilization of iron-containing mineral dust to improvement of air quality projected in the future, *Atmos. Chem. Phys.*, 14, 3441–3459, doi:10.5194/acp-14-3441-2014, 2014.

**Anthropogenic
bioavailable Fe
deposition**

A. Ito and Z. Shi

Title Page

Abstract

Introduction

Conclusions

References

Tables

Figures



Back

Close

Full Screen / Esc

Printer-friendly Version

Interactive Discussion



- Ito, A., Kok, J., Feng, Y., and Penner, J.: Does a theoretical estimation of the dust size distribution at emission suggest more bioavailable iron deposition?, *Geophys. Res. Lett.*, 39, L05807, doi:10.1029/2011GL050455, 2012.
- Ito, A., Lin, G., Penner, J. E.: Reconciling modeled and observed atmospheric deposition of soluble organic nitrogen at coastal locations, *Global Biogeochem. Cy.*, 28, 617–630, doi:10.1002/2013GB004721, 2014.
- Ito, A., Lin, G., and Penner, J. E.: Global modeling study of soluble organic nitrogen from open biomass burning, *Atmos. Environ.*, doi:10.1016/j.atmosenv.2015.01.031, in press, 2015.
- Jang, J. H., Dempsey, B. A., and Burgos, W. D.: Solubility of hematite revisited: effects of hydration, *Environ. Sci. Technol.*, 41, 7303–7308, doi:10.1021/es8010139, 2007.
- Jickells, T. D., An, Z. S., Andersen, K. K., Baker, A. R., Bergametti, G., Brooks, N., Cao, J. J., Boyd, P. W., Duce, R. A., Hunter, K. A., Kawahata, H., Kubilay, N., LaRoche, J., Liss, P. S., Mahowald, N., Prospero, J. M., Ridgwell, A. J., Tegen, I., and Torres, R.: Global iron connections between desert dust, ocean biogeochemistry, and climate, *Science*, 308, 67–71, doi:10.1126/science.1105959, 2005.
- Johnson, M. S. and Meskhidze, N.: Atmospheric dissolved iron deposition to the global oceans: effects of oxalate-promoted Fe dissolution, photochemical redox cycling, and dust mineralogy, *Geosci. Model Dev.*, 6, 1137–1155, doi:10.5194/gmd-6-1137-2013, 2013.
- Johnson, M. S., Meskhidze, N., Solmon, F., Gassó, S., Chuang, P. Y., Gaiero, D. M., Yantosca, R. M., Wu, S., Wang, Y., and Carouge, C.: Modeling dust and soluble iron deposition to the South Atlantic Ocean, *J. Geophys. Res.*, 115, D15202, doi:10.1029/2009JD013311, 2010.
- Journet, E., Desboeufs, K. V., Caquineau, S., and Colin, J.-L.: Mineralogy as a critical factor of dust iron solubility, *Geophys. Res. Lett.*, 35, L07805, doi:10.1029/2007GL031589, 2008.
- Journet, E., Balkanski, Y., and Harrison, S. P.: A new data set of soil mineralogy for dust-cycle modeling, *Atmos. Chem. Phys.*, 14, 3801–3816, doi:10.5194/acp-14-3801-2014, 2014.
- Kok, J. F.: A scaling theory for the size distribution of emitted dust aerosols suggests climate models underestimate the size of the global dust cycle, *P. Natl. Acad. Sci. USA*, 108, 1016–1021, doi:10.1073/pnas.1014798108, 2011.
- Kraemer, S. M. and Hering, J. G.: Influence of solution saturation state on the kinetics of ligand-controlled dissolution of oxide phases, *Geochim. Cosmochim. Ac.*, 61, 2855–2866, 1997.
- Lamarque, J.-F., Bond, T. C., Eyring, V., Granier, C., Heil, A., Klimont, Z., Lee, D., Liousse, C., Mieville, A., Owen, B., Schultz, M. G., Shindell, D., Smith, S. J., Stehfest, E., Van Aar-

**Anthropogenic
bioavailable Fe
deposition**

A. Ito and Z. Shi

Title Page

Abstract

Introduction

Conclusions

References

Tables

Figures



Back

Close

Full Screen / Esc

Printer-friendly Version

Interactive Discussion



denne, J., Cooper, O. R., Kainuma, M., Mahowald, N., McConnell, J. R., Naik, V., Riahi, K., and van Vuuren, D. P.: Historical (1850–2000) gridded anthropogenic and biomass burning emissions of reactive gases and aerosols: methodology and application, *Atmos. Chem. Phys.*, 10, 7017–7039, doi:10.5194/acp-10-7017-2010, 2010.

5 Lanzl, C. A., Baltrusaitis, J., and Cwienty, D. M.: Dissolution of hematite nanoparticle aggregates: influence of primary particle size, dissolution mechanism, and solution pH, *Langmuir*, 28, 15797–15808, doi:10.1021/la3022497, 2012.

Lasaga, A. C., Soler, J. M., Ganor, J., Burch, T. E., and Nagy, K. L.: Chemical-weathering rate laws and global geochemical cycles, *Geochim. Cosmochim. Ac.*, 58, 2361–2386, 1994.

10 Lin, G., Sillman, S., Penner, J. E., and Ito, A.: Global modeling of SOA: the use of different mechanisms for aqueous-phase formation, *Atmos. Chem. Phys.*, 14, 5451–5475, doi:10.5194/acp-14-5451-2014, 2014.

Liu, X., Penner, J. E., and Herzog, M.: Global modeling of aerosol dynamics: model description, evaluation and interactions between sulfate and non-sulfate aerosols, *J. Geophys. Res.*, 110, D18206, doi:10.1029/2004JD005674, 2005.

15 Lowson, R. T., Comarmond, M. C. J., Rajaratnam, G., and Brown, P. L.: The kinetics of the dissolution of chlorite as a function of pH and at 25 °C, *Geochim. Cosmochim. Ac.*, 69, 1687–1699, doi:10.1016/j.gca.2004.09.028, 2005.

Luo, C. and Gao, Y.: Aeolian iron mobilisation by dust-acid interactions and their implications for soluble iron deposition to the ocean: a test involving potential anthropogenic organic acidic species, *Environ. Chem.*, 7, 153–161, doi:10.1071/EN09116, 2010.

20 Luo, C., Mahowald, N., Bond, T., Chuang, P. Y., Artaxo, P., Siefert, R., Chen, Y., and Schauer, J.: Combustion iron distribution and deposition, *Global Biogeochem. Cy.*, 22, GB1012, doi:10.1029/2007GB002964, 2008.

25 Mackie, D. S., Boyd, P. W., Hunter, K. A., and McTainsh, G. H.: Simulating the cloud processing of iron in Australian dust: pH and dust concentration, *Geophys. Res. Lett.*, 32, L06809, doi:10.1029/2004GL022122, 2005.

Mahowald, N. M., Engelstaedter, S., Luo, C., Sealy, A., Artaxo, P., Benitez-Nelson, C., Bonnet, S., Chen, Y., Chuang, P. Y., Cohen, D. D., Dulac, F., Herut, B., Johansen, A. M., Kubilay, N., Losno, R., Maenhaut, W., Paytan, A., Prospero, J. A., Shank, L. M., and Siefert, R. L.: Atmospheric iron deposition: global distribution, variability, and human perturbations, *Annu. Rev. Mar. Sci.*, 1, 245–278, doi:10.1146/annurev.marine.010908.163727, 2009.

**Anthropogenic
bioavailable Fe
deposition**

A. Ito and Z. Shi

Title Page

Abstract

Introduction

Conclusions

References

Tables

Figures



Back

Close

Full Screen / Esc

Printer-friendly Version

Interactive Discussion



- Malmström, M. and Banwart, S.: Biotite dissolution at 25 °C: the pH dependence of dissolution rate and stoichiometry, *Geochim. Cosmochim. Ac.*, 61, 2779–2799, 1997.
- Meskhidze, N., Chameides, W. L., Nenes, A., and Chen, G.: Iron mobilization in mineral dust: can anthropogenic SO₂ emissions affect ocean productivity?, *Geophys. Res. Lett.*, 30, 2085, doi:10.1029/2003GL018035, 2003.
- Meskhidze, N., Chameides, W. L., and Nenes, A.: Dust and pollution: a recipe for enhanced ocean fertilization?, *J. Geophys. Res.*, 110, D03301, doi:10.1029/2004JD005082, 2005.
- Myriokefalitakis, S., Daskalakis, N., Mihalopoulos, N., Baker, A. R., Nenes, A., and Kanakidou, M.: Changes in dissolved iron deposition to the oceans driven by human activity: a 3-D global modelling study, *Biogeosciences*, 12, 3973–3992, doi:10.5194/bg-12-3973-2015, 2015.
- Parazols, M., Marinoni, A., Amato, P., Abida, O., Laj, P., and Mailhot, G.: Speciation and role of iron in cloud droplets at the puy de Dôme station, *J. Atmos. Chem.*, 54, 267–281, doi:10.1007/s10874-006-9026-x, 2006.
- Paris, R., Desboeufs, K. V., and Journet, E.: Variability of dust iron solubility in atmospheric waters: investigation of the role of oxalate organic complexation, *Atmos. Environ.*, 45, 6510–6517, doi:10.1016/j.atmosenv.2011.08.068, 2011.
- Ramos, M. E., García-Palma, S., Rozalén, M., Johnston, C. T., and Huertas, F. J.: Kinetics of montmorillonite dissolution: an experimental study of the effect of oxalate, *Chem. Geol.*, 363, 283–292, doi:10.1016/j.chemgeo.2013.11.014, 2014.
- Rotman, D. A., Atherton, C. S., Bergmann, D. J., Cameron-Smith, P. J., Chuang, C. C., Connell, P. S., Dignon, J. E., Franz, A., Grant, K. E., Kinnison, D. E., Molenkamp, C. R., Proctor, D. D., and Tannahill, J. R.: IMPACT, the LLNL 3-D global atmospheric chemical transport model for the combined troposphere and stratosphere: model description and analysis of ozone and other trace gases, *J. Geophys. Res.*, 109, D04303, doi:10.1029/2002JD003155, 2004.
- Rozalén, M. L., Huertas, F. J., Brady, P. V., Cama, J., García-Palma, S., and Linares, J.: Experimental study of the effect of pH on the kinetics of montmorillonite dissolution at 25 °C, *Geochim. Cosmochim. Ac.*, 72, 4224–4253, doi:10.1016/j.gca.2008.05.065, 2008.
- Rozalén, M., Ramos, M. E., Fiore, S., Gervilla, F., and Huertas, F. J.: Effect of oxalate and pH on chrysotile dissolution at 25 °C: an experimental study, *Am. Mineral.*, 99, 589–600, doi:10.2138/am.2014.4636, 2014.

**Anthropogenic
bioavailable Fe
deposition**

A. Ito and Z. Shi

Title Page

Abstract

Introduction

Conclusions

References

Tables

Figures



Back

Close

Full Screen / Esc

Printer-friendly Version

Interactive Discussion



Rubasinghege, G., Lentz, R. W., Scherer, M. M., and Grassian, V. H.: Simulated atmospheric processing of iron oxyhydroxide minerals at low pH: roles of particle size and acid anion in iron dissolution, *P. Natl. Acad. Sci. USA*, 107, 6628–6633, doi:10.1073/pnas.0910809107, 2010.

5 Scanza, R. A., Mahowald, N., Ghan, S., Zender, C. S., Kok, J. F., Liu, X., Zhang, Y., and Albani, S.: Modeling dust as component minerals in the Community Atmosphere Model: development of framework and impact on radiative forcing, *Atmos. Chem. Phys.*, 15, 537–561, doi:10.5194/acp-15-537-2015, 2015.

10 Sedwick, P. N., Sholkovitz, E. R., and Church, T. M.: Impact of anthropogenic combustion emissions on the fractional solubility of aerosol iron: evidence from the Sargasso Sea, *Geochem. Geophys. Geosy.*, 8, Q10Q06, doi:10.1029/2007GC001586, 2007.

15 Séguret, M. J. M., Koçak, M., Theodosi, C., Ussher, S. J., Worsfold, P. J., Herut, B., Mihalopoulos, N., Kubilay, N., and Nimmo, M.: Iron solubility in crustal and anthropogenic aerosols: the Eastern Mediterranean as a case study, *Mar. Chem.*, 126, 229–238, doi:10.1016/j.marchem.2011.05.007, 2011.

Shi, Z., Krom, M. D., Bonneville, S., Baker, A. R., Jickells, T. D., and Benning, L. G.: Formation of iron nanoparticles and increase in iron reactivity in the mineral dust during simulated cloud processing, *Environ. Sci. Technol.*, 43, 6592–6596, doi:10.1021/es901294g, 2009.

20 Shi, Z., Bonneville, S., Krom, M. D., Carslaw, K. S., Jickells, T. D., Baker, A. R., and Benning, L. G.: Iron dissolution kinetics of mineral dust at low pH during simulated atmospheric processing, *Atmos. Chem. Phys.*, 11, 995–1007, doi:10.5194/acp-11-995-2011, 2011.

25 Shi, Z., Krom, M. D., Jickells, T. D., Bonneville, S., Carslaw, K. S., Mihalopoulos, N., Baker, A. R., and Benning, L. G.: Impacts on iron solubility in the mineral dust by processes in the source region and the atmosphere: a review, *Aeolian Res.*, 5, 21–42, doi:10.1016/j.aeolia.2012.03.001, 2012.

Shi, Z., Krom, M. D., Bonneville, S., and Benning, L. G.: Atmospheric processing outside clouds increases soluble iron in mineral dust, *Environ. Sci. Technol.*, 49, 1472–1477, doi:10.1021/es504623x, 2015.

30 Solmon, F., Chuang, P. Y., Meskhidze, N., and Chen, Y.: Acidic processing of mineral dust iron by anthropogenic compounds over the north Pacific Ocean, *J. Geophys. Res.*, 114, D02305, doi:10.1029/2008JD010417, 2009.

Spokes, J. L. and Jickells, T. D: Factors controlling the solubility of aerosol trace metals in the atmosphere and on mixing into seawater, *Aquat. Geochem.*, 1, 355–374, 1996.

**Anthropogenic
bioavailable Fe
deposition**

A. Ito and Z. Shi

Title Page

Abstract

Introduction

Conclusions

References

Tables

Figures



Back

Close

Full Screen / Esc

Printer-friendly Version

Interactive Discussion



Wang, R., Balkanski, Y., Boucher, O., Bopp, L., Chappell, A., Ciais, P., Hauglustaine, D., Peñuelas, J., and Tao, S.: Sources, transport and deposition of iron in the global atmosphere, *Atmos. Chem. Phys.*, 15, 6247–6270, doi:10.5194/acp-15-6247-2015, 2015.

Wexler, A. S. and Clegg, S. L.: Atmospheric aerosol models for systems including the ions H^+ , NH_4^+ , Na^+ , SO_4^{2-} , NO_3^- , Cl^- , Br^- , and H_2O , *J. Geophys. Res.* 107, 4207, doi:10.1029/2001jd000451, 2002.

Wozniak, A. S., Shelley, R. U., Sleighter, R. L., Abdulla, H. A. N., Morton, P. L., Landing, W. M., and Hatcher, P. G.: Relationships among aerosol water soluble organic matter, iron and aluminum in European, North African, and Marine air masses from the 2010 US GEOTRACES cruise, *Mar. Chem.*, 153, 24–33, doi:10.1016/j.marchem.2013.04.011, 2013.

Wozniak, A. S., Shelley, R. U., McElhenie, S. D., Landing, W. M., and Hatcher, P. G.: Aerosol water soluble organic matter characteristics over the North Atlantic Ocean: implications for iron-binding ligands and iron solubility, *Mar. Chem.*, 173, 162–172, doi:10.1016/j.marchem.2014.11.002, 2015.

Xu, L. and Penner, J. E.: Global simulations of nitrate and ammonium aerosols and their radiative effects, *Atmos. Chem. Phys.*, 12, 9479–9504, doi:10.5194/acp-12-9479-2012, 2012.

Xu, N. and Gao, Y.: Characterization of hematite dissolution affected by oxalate coating, kinetics and pH, *Appl. Geochem.*, 23, 783–793, doi:10.1016/j.apgeochem.2007.12.026, 2008.

Yoon, T. H., Johnson, S. B., Musgrave, C. B., and Brown, G. E.: Adsorption of organic matter at mineral/water interfaces: I. ATR-FTIR spectroscopic and quantum chemical study of oxalate adsorbed at boehmite/water and corundum/water interfaces, *Geochim. Cosmochim. Ac.*, 68, 4505–4518, doi:10.1016/j.gca.2004.04.025, 2004.

Yu, J. Z., Huang, X.-F., Xu, J., and Hu, M.: When aerosol sulfate goes up, so does oxalate: implication for the formation mechanisms of oxalate, *Environ. Sci. Technol.*, 39, 128–133, doi:10.1021/es049559f, 2005.

Zhang, Y., Kallay, N., and Matijević, E.: Interactions of metal hydrous oxides with chelating agents. 7. Hematite-oxalic acid and -citric acid systems, *Langmuir*, 1, 201–206, 1985.

Zhuang, G., Yi, Z., Duce, R. A., and Brown, P. R.: Link between iron and sulphur cycles suggested by detection of Fe(II) in remote marine aerosols, *Nature*, 355, 537–539, 1992.

Anthropogenic bioavailable Fe deposition

A. Ito and Z. Shi

Table 1. Global Fe emission (Fe Tg yr^{-1}) estimated for different types of Fe-containing aerosols.

Species	Preindustrial era	Present day
Dust	69 (98 %)	69 (98 %)
Oil combustion	0 (0 %)	0.022 (0.03 %)
Coal combustion	0.28 (1.0 %)	0.69 (1.0 %)
Biomass burning	0.66 (0.9 %)	0.66 (0.9 %)
Total Fe	70	71

Note: the parentheses represent the percentage of each source of Fe to total Fe. The initial Fe solubility ($58 \pm 22\%$) is used to estimate primary soluble Fe emission for the oil combustion aerosols only (Ito, 2015). Insoluble Fe can be transformed to secondary soluble Fe via atmospheric processing of iron-containing mineral dust (see the text) and combustion aerosols (Ito, 2015).

[Title Page](#)
[Abstract](#)
[Introduction](#)
[Conclusions](#)
[References](#)
[Tables](#)
[Figures](#)

[Back](#)
[Close](#)
[Full Screen / Esc](#)
[Printer-friendly Version](#)
[Interactive Discussion](#)


Anthropogenic
bioavailable Fe
deposition

A. Ito and Z. Shi

Title Page

Abstract

Introduction

Conclusions

References

Tables

Figures



Back

Close

Full Screen / Esc

Printer-friendly Version

Interactive Discussion

**Table 2.** Constants used to calculate Fe dissolution rates for mineral dust, based on laboratory experiments.

Stage	Species	Scheme	Rate Constant k_i (pH, T) ¹	m_i^3	K_{eq}^4	n_i^5
I	Ferrihydrite	Proton	$7.13 \times 10^{-5} \exp[E(\text{pH})^2 \times (1/298 - 1/T)]$	1.1	1550	3
II	Nano-Fe oxides	Proton	$1.43 \times 10^{-4} \exp[E(\text{pH})^2 \times (1/298 - 1/T)]$	1.6	42	2.75
III	Aluminosilicates	Proton	$5.85 \times 10^{-8} \exp[E(\text{pH})^2 \times (1/298 - 1/T)]$	0.76	3.3	2.85
I	Ferrihydrite	Oxalate	$4.61 \times 10^{-8} \exp[E(\text{pH})^2 \times (1/298 - 1/T)]$	0.069	1550^6	3^6
II	Nano-Fe oxides	Oxalate	$1.28 \times 10^{-8} \exp[E(\text{pH})^2 \times (1/298 - 1/T)]$	0.069	1550^6	3^6
III	Aluminosilicates	Oxalate	$1.68 \times 10^{-9} \exp[E(\text{pH})^2 \times (1/298 - 1/T)]$	0.056	1550^6	3^6
I	Ferrihydrite	Phot	$4.61 \times 10^{-8} \exp[E(\text{pH})^2 \times (1/298 - 1/T)]$	0.069		
II	Nano-Fe oxides	Phot	$1.28 \times 10^{-8} \exp[E(\text{pH})^2 \times (1/298 - 1/T)]$	0.069		
III	Aluminosilicates	Phot	$1.68 \times 10^{-9} \exp[E(\text{pH})^2 \times (1/298 - 1/T)]$	0.056		

¹ k_i (pH, T) is the pH- and temperature-dependent “far-from-equilibrium” Fe dissolution rate of Fe-containing mineral dust (moles Fe $\text{g}^{-1} \text{s}^{-1}$) for each Fe dissolution scheme i . The parameters are fit to our measurements for African dust. The photo-induced dissolution rate of Fe compounds is scaled to the photolysis rate of H_2O_2 calculated in the model, following Ito (2015).

² $E(\text{pH}) = -1.56 \times 10^3 \times \text{pH} + 1.08 \times 10^4$. The parameters are fit to the measurements for soils (Bibi et al., 2014).

³ m_i is the reaction order with respect to aqueous phase protons, which was determined by linear regression from our experimental data in the pH range between 2 and 3 for proton- and oxalate-promoted dissolution schemes.

⁴ K_{eq} is the equilibrium constant ($\text{mol}^2 \text{kg}^{-2}$) (Bonneville et al., 2004; Jang et al., 2007).

⁵ n_i is the stoichiometric ratio (Bonneville et al., 2004; Jang et al., 2007).

⁶ The formation of the amorphous $\text{Fe}(\text{OH})_3(\text{s})$ suppresses the oxalate-promoted dissolution from mineral aerosols in the base simulations, while no such effect was considered for quasi-light-induced reductive dissolution in the sensitivity simulation (i.e., $f_3 = 1$).

Anthropogenic bioavailable Fe deposition

A. Ito and Z. Shi

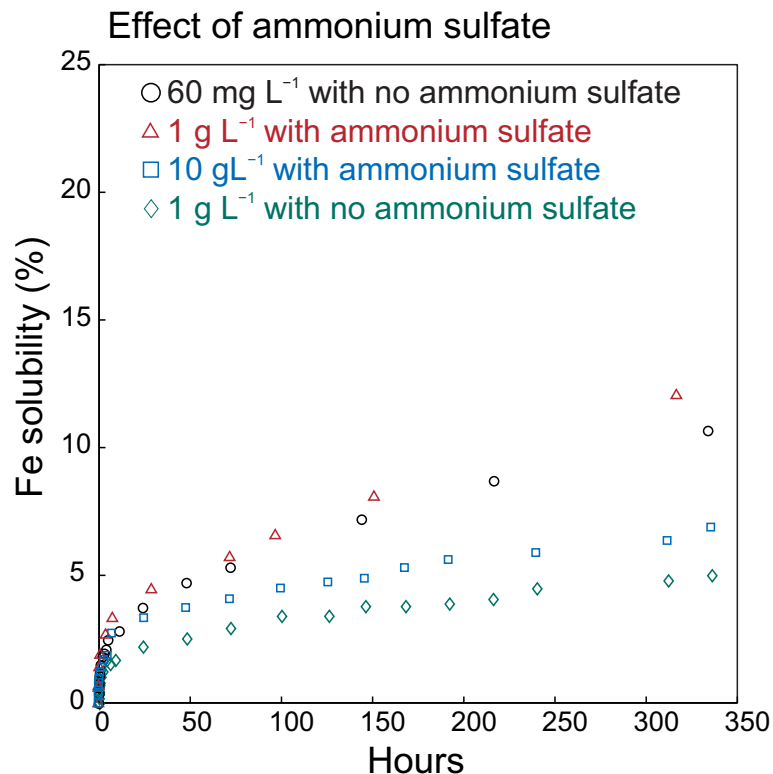


Figure 1. Comparison of Fe solubility in solution (%) measured at two different dust/liquid ratios of 1 g L^{-1} (red triangles) and 10 g L^{-1} (blue squares) in 0.05 mol L^{-1} sulfuric acid solution with 1 mol L^{-1} $(\text{NH}_4)_2\text{SO}_4$ ($I = 3.15 \text{ mol kg}^{-1}$), and dust/liquid ratios of 60 mg L^{-1} (black circles) and 1 g L^{-1} (green diamonds) in 0.005 mol L^{-1} sulfuric acid solution without $(\text{NH}_4)_2\text{SO}_4$ ($\text{pH} = 2.0$).

Anthropogenic
bioavailable Fe
deposition

A. Ito and Z. Shi

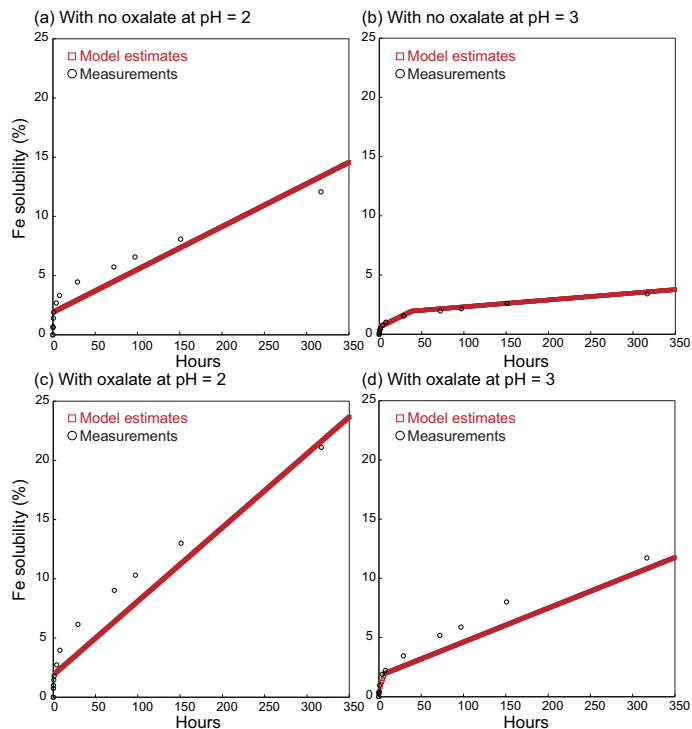


Figure 2. Comparison of Fe solubility in solution (%) predicted using Eq. (1) with our measured Fe dissolution rates **(a)** with no oxalate at pH = 2, 0.05 M H_2SO_4 , 1 M $(\text{NH}_4)_2\text{SO}_4$, **(b)** with no oxalate at pH = 3, 0.005 M H_2SO_4 , 1 M $(\text{NH}_4)_2\text{SO}_4$, **(c)** with oxalate at pH = 2.1, 0.05 M H_2SO_4 , 1 M $(\text{NH}_4)_2\text{SO}_4$, and 0.03 M $\text{Na}_2\text{C}_2\text{O}_4$, **(d)** with oxalate at pH = 3, 0.005 M H_2SO_4 , 1 M $(\text{NH}_4)_2\text{SO}_4$, and 0.03 M $\text{Na}_2\text{C}_2\text{O}_4$. The red squares are calculated using Eq. (1) from the rate constants used in this study at each hour. The black circles are our measured data. The values of pH in solution are calculated using E-AIM (Wexler and Clegg, 2002, <http://www.aim.env.uea.ac.uk/aim/aim.php>).

Title Page

Abstract

Introduction

Conclusions

References

Tables

Figures



Back

Close

Full Screen / Esc

Printer-friendly Version

Interactive Discussion



Anthropogenic
bioavailable Fe
deposition

A. Ito and Z. Shi

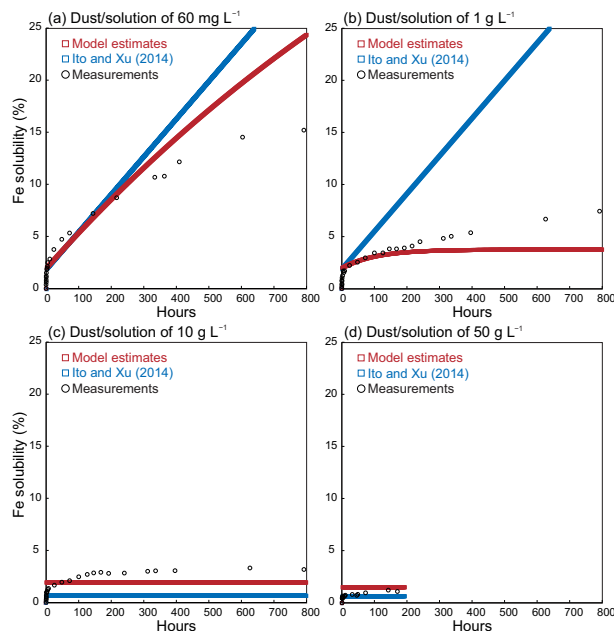


Figure 3. Comparison of Fe solubility in solution (%) predicted using Eq. (1) with the measured Fe dissolution rates at pH = 2, 0.005 M H₂SO₄, and dust/solution of (a) 60 mg L⁻¹, (b) 1 g L⁻¹, (c) 10 g L⁻¹, and (d) 50 g L⁻¹. The red squares are calculated using Eq. (1) from the equilibrium constant (mol² kg⁻²) used in this study at each hour. The blue squares are calculated using Eq. (1) from the equilibrium constant (mol² kg⁻²) used in Ito and Xu (2014). The black circles are our measured data. The fraction of total dissolved Fe present as Fe(III) is prescribed at pH = 2 (0.2) in this calculation to emulate the experimental conditions, while the photochemical redox cycling between Fe(III) and Fe(II) in solution is explicitly simulated in our global model (Lin et al., 2014). The large fraction of Fe(II) in solution under the dark conditions is likely associated with the Fe dissolution of Fe(II)-containing solids (Cwienty et al., 2008). The initial fraction of Fe speciation is not critical in estimating the Fe redox speciation in aerosol water, because Fe(II) is quickly oxidized to Fe(III) in oxygenated water (Deguillaume et al., 2010).

Title Page

Abstract

Introduction

Conclusions

References

Tables

Figures



Back

Close

Full Screen / Esc

Printer-friendly Version

Interactive Discussion



Anthropogenic
bioavailable Fe
deposition

A. Ito and Z. Shi

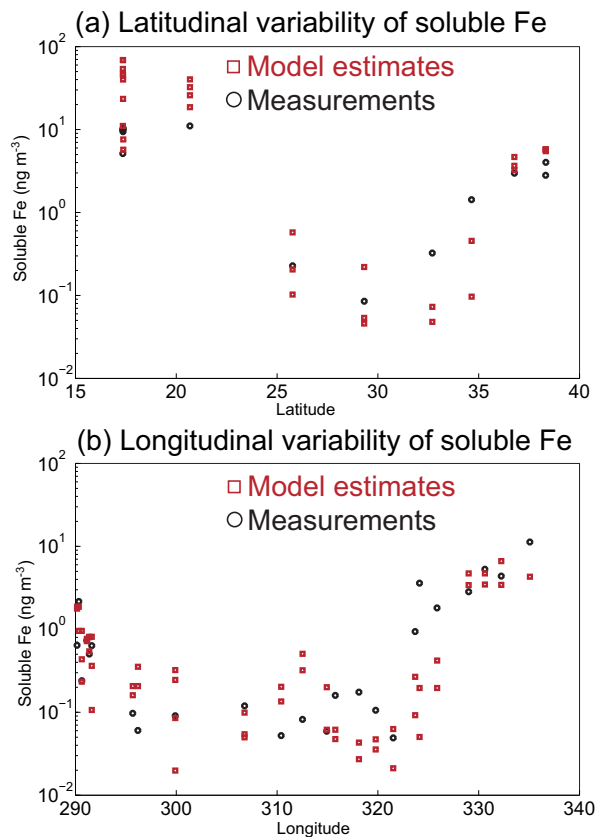


Figure 4. Comparison of simulated (red squares) and observed (black circles) soluble Fe concentration (ng m⁻³) during **(a)** 2010 and **(b)** 2011 US GEOTRACES cruise over the North Atlantic (Wozniak et al., 2013, 2015). The number of modeled data points (84) is larger than the measurements (37), because each daily average is calculated for each sampling date at each center of cruise location.

Anthropogenic bioavailable Fe deposition

A. Ito and Z. Shi

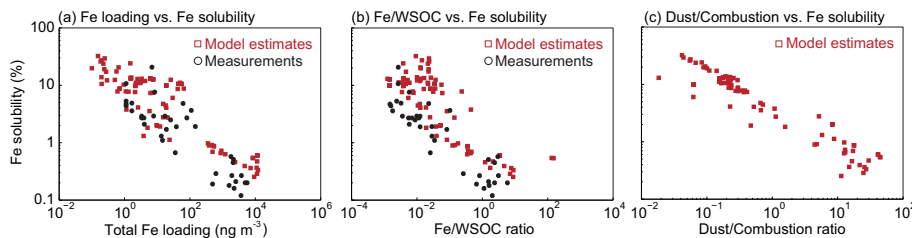


Figure 5. (a) Atmospheric loading of total aerosol Fe (ng m^{-3}) vs. Fe solubility for model estimates (red squares) and measurements (black circles) over the cruise tracks. (b) The Fe/WSOC molar ratio vs. Fe solubility for model estimates (red squares) and measurements (black circles) over the cruise tracks. (c) The dust/combustion ratio for soluble Fe vs. percent of soluble Fe in total Fe for model results over the cruise tracks. The measurements are obtained from Wozniak et al. (2013, 2015). The number of modeled data points (84) is larger than the measurements (37), because each daily average is calculated for each sampling date at each center of cruise location.

Title Page

Abstract

Introduction

Conclusions

References

Tables

Figures

◀

▶

◀

▶

Back

Close

Full Screen / Esc

Printer-friendly Version

Interactive Discussion



Anthropogenic
bioavailable Fe
deposition

A. Ito and Z. Shi

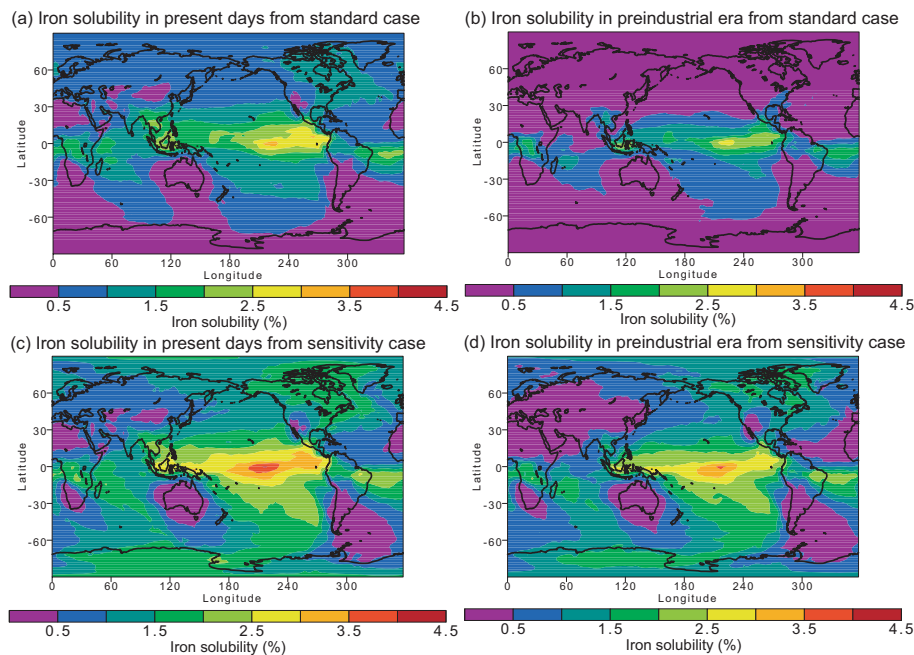


Figure 6. Ratio (%) of the soluble to total Fe deposition for mineral dust in **(a)** present days from base simulations, **(b)** preindustrial era from base simulations, **(c)** present days from sensitivity simulations, and **(d)** preindustrial era from sensitivity simulations. The formation of the amorphous $\text{Fe}(\text{OH})_3(\text{s})$ suppresses the oxalate-promoted dissolution from mineral aerosols in the base simulations, while no such effect was considered for quasi-light-induced reductive dissolution in the sensitivity simulation (i.e., $f_3 = 1$).

